IEEE Access
Multidisciplinary | Rapid Review | Open Access Journal

Received February 21, 2022, accepted March 10, 2022, date of publication March 16, 2022, date of current version March 22, 2022.

Digital Object Identifier 10.1109/ACCESS.2022.3159801

Solar Power Generation System With Power Smoothing Function

JINN-CHANG WU[1], (Member, IEEE), HURNG-LIAHNG JOU[2], (Member, IEEE), WEN-CHAN WU[1], AND CHUNG-HSUN CHANG[1]

[1]Department of Microelectronics Engineering, National Kaohsiung University of Science and Technology, Kaohsiung 81157, Taiwan
[2]Department of Electrical Engineering, National Kaohsiung University of Science and Technology, Kaohsiung 81157, Taiwan

Corresponding author: Jinn-Chang Wu (jinnwu@nkust.edu.tw)

This work was supported in part by the Ministry of Science and Technology of Taiwan under Contract MOST 109-2221-E-992-028.

ABSTRACT The output power from a solar power generation system (SPGS) changes significantly because of environmental factors, which affects the stability and reliability of a power distribution system. This study proposes a SPGS with the power smoothing function. The proposed SPGS consists of a solar cell array, a battery set, a dual-input buck-boost DC-AC inverter (DIBBDAI) and a boost power converter (BPC). The DIBBDAI combines the functions of voltage boost, voltage buck and DC-AC power conversion. The BPC acts as a battery charger between the solar cell array and the battery set. For the proposed SPGS, the DC power that is provided by the solar cell array or the battery set is converted into AC power through only one power stage. The solar cell array also charges the battery set through only one power stage. This increases the power conversion efficiency for the solar cell array, the battery set and the utility. The battery set is charged/discharged when the output power of the solar cell array changes drastically, in order to smooth the output power from the SPGS. In addition, the DIBBDAI can suppress the leakage current that is induced by the parasitic capacitance of the solar cell array. The proposed power conversion interface increases power efficiency, smooths power fluctuation and decreases leakage current for a SPGS. A hardware prototype is completed to verify the performance of the proposed SPGS.

INDEX TERMS Solar power generation, power smoothing, buck-boost DC-AC inverter.

I. INTRODUCTION

Extreme climate change has created global warming. In order to prevent irreversible climate change, the United Nations promotes the international convention on greenhouse gas emission reduction. Most countries are actively developing renewable power generation to reduce the environmental impact of greenhouse gas emissions. Renewable energy from solar energy and wind energy involves mature technology and is widely used to generate electricity. In the past, renewable power generation was expensive and depended on government subsidies but the cost of renewable power generation has decreased rapidly due to developments in manufacturing technology. The cost of renewable energy power generation in many countries is close to or less than the price of electricity that is generated using fossil fuels so an increasing number of renewable power generation systems are being integrated into the grid to generate electricity.

The associate editor coordinating the review of this manuscript and approving it for publication was Sze Sing Lee.

The output power from a solar power generation system (SPGS) changes significantly due to environmental factors [1]–[12]. These environmental factors change with the weather and seasons and cannot be controlled. As the penetration of SPGSs increases, drastic changes in their power generation will affect the voltage and frequency of distribution power system and can cause power outages. This reduces the power quality of distribution power systems.

Several control strategies for the power conversion interface are used to alleviate the fluctuation in the output power from a SPGS [1]. However, these control strategies only limit the increase in power from the SPGS by giving up maximum power tracking, and they only suppress the upward power fluctuations for the SPGS. In addition, the power that is generated by the SPGS is also decreased. To suppress upward and downward fluctuations of the SPGS, the rapid power regulation technology is required to temporarily store and release power to stabilize the power output from the SPGS. Since battery set has the advantages of small size, quick absorption and release of electrical energy and flexible operation, it has

considerable potential as a power regulation device for the SPGS [2]–[16]. In general, the control concept for smoothing the output power of SPGS is that the battery energy storage system supplies the difference between the average value and the instantaneous value for the output power of SPGS. The average value for the output power of SPGS can be calculated by low-pass filters [3]–[6], moving average filters [3], [4], [7], Saviztky–Golay filtering [8] and moving regression filter [9]. Since the instantaneous value for the output power of SPGS is rare equal to its average value, the charging/discharging time of the battery set is long.

The output from a solar cell array is DC power and the battery set stores power in DC form, so a power conversion interface is needed for integrating solar cell array or battery set into the power grid for DC-AC power conversion [1]–[23]. The configuration of SPGS and battery energy storage system can be divided into AC coupling [9]–[12] and DC coupling [4], [8], [13]–[16]. For the AC coupling configuration, the SPGS and the battery energy storage system (BESS) are respectively connected to the grid. Therefore, the SPGS and the BESS have their own DC-AC power converter and the circuit structure is more complicated. For the DC coupling configuration, the SPGS and the BESS share a common DC-AC power converter so the circuit structure is relatively simple.

Small capacity SPGSs or BESS use fewer solar modules or batteries so the DC voltage is lower. A DC-AC power converter with a traditional bridge architecture or multi-level architecture is derived from a buck power converter so the DC bus voltage for the DC-AC power converter must be greater than the peak value of grid voltage [1]–[18]. A boost power converter (BPC) must be inserted between the DC-AC power converter and the solar cell array or battery set and all power from the solar cell array or battery set must be processed using two power conversion stages. For the AC coupling configuration of SPGS and battery energy storage system, it needs four power stages for power conversion. The number of power processing stage is reduced to three for the DC coupling configuration of SPGS and battery energy storage system. Hence, the power circuit is more complicated and the power efficiency is degraded. In addition, the charging power from solar cell array to the battery set should also be processed using two DC-DC power converters for integrating the BESS to perform the power smoothing function for a SPGS

An Z-source DC-AC power converter shifts the filter inductor from the AC side of the traditional bridge architecture to the DC side so the power electronic switches for the same arm in the bridge architecture can be turned on at the same time to boost the voltage [19], [20], [24], [25]. As a result, the DC input voltage can be less than the peak value of grid voltage. However, the boosting voltage gain is limited and the control is more complicated. A boost DC-AC power converter uses two BPCs for DC-AC power conversion [26], [27]. Each BPC generates an AC voltage with a DC offset. The output voltage is the difference between the output voltages of the two BPCs and the DC offsets will be canceled each other. However, the output voltage has a higher peak value due to the DC offset. As a result, the voltage rating and the switching loss for the power electronic switches are increased. In addition, the Z-source DC-AC power converter and the boost DC-AC power converter cannot solve the problem of leakage current for the applications of SPGS. In [28], [29], a buck-boost converter is integrated to the AC side of bridge architecture. The bridge architecture is switched in synchronous with the grid voltage to generate a square voltage, and the buck-boost converter is used to step up or down voltage and control the output current. The bridge architecture can be replaced by cascaded bridge architecture [30]. The power electronic switches used in the buck-boost converter should be bidirectional, which are composed of two conventional power electronic switches in series. The buck-boost converter can also be integrated to the DC side of bridge architecture [31], [32]. However, the power efficiency for the buck-boost converter is degraded because all of conversion power should be stored to and then released from the inductor. Moreover, these DC-AC power converters process only one DC power source.

This study proposes a SPGS with a power smoothing function. The proposed SPGS uses a dual-input buck-boost DC-AC inverter (DIBBDAI) and a BPC to integrate a solar cell array and a battery set to generate power injecting into the grid. The DIBBDAI integrates two DC power sources. For the proposed SPGS, the DC power that is provided by either the solar cell array or the battery set is converted into AC power using only the DIBBDAI, and the battery set is charged from the solar cell array only using the BPC. The battery set is charged/discharged when the output power from the solar cell array changes significantly, in order to smooth the output power from the SPGS. The negative terminal voltage for the solar cell array contains little high frequency components, so the leakage current that is induced by the parasitic capacitance of the solar cell array is smaller.

This paper is organized as follows. In Section II, the circuit configuration is presented. In Sections III and IV, the operations of the DIBBDAI and BPC are addressed. The operation flowchart for the proposed SPGS with power smoothing function is explained in Section V. The control block for DIBBDAI is introduced in Section VI. In Section VII, several experimental results are provided to verify the proposed SPGS. Finally, some conclusions are summarized in Section VIII.

II. CIRCUIT CONFIGURATION

The circuit configuration for the proposed SPGS is shown in Fig. 1. The DC coupling configuration is used for the proposed SPGS. As seen in Fig. 1, the proposed SPGS is composed of a solar cell array, a battery set and the power conversion interface. The power conversion interface consists of a DIBBDAI and a BPC. The BPC is connected between the solar cell array and the battery set to control the power from the solar cell array that charges the battery set. In order to reduce the capacity of battery set, the battery set only operates when the power variation for the solar cell array exceeds the

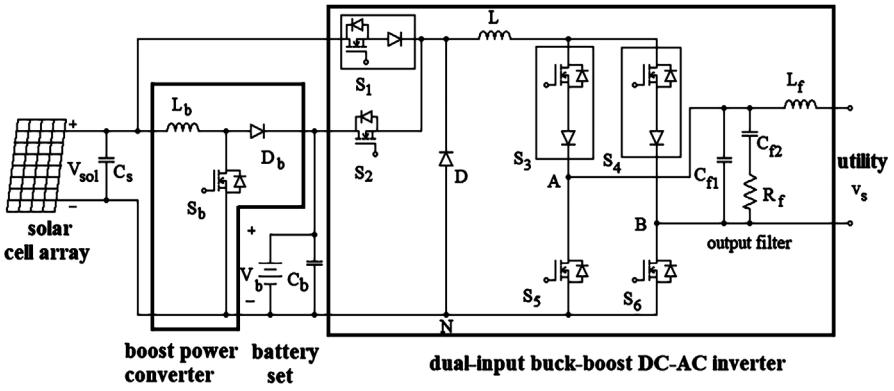

FIGURE 1. Circuit configuration for the proposed SPGS.

specified range. The battery set is only charged by the solar cell array so the power flow of BPC is unidirectional.

The DIBBDAI performs the functions of voltage boost, voltage buck and DC-AC power conversion. The DIBBDAI BPC operate at the same time to convert the power from the solar cell array for injecting into the grid and for charging the battery set, respectively.

III. OPERATION OF DIBBDAI

The two input terminals of the DIBBDAI are respectively connected to the solar cell array and the battery set. The operation of the DIBBDAI can be divided into the boost mode and the buck mode. The two input terminals of the DIBBDAI are respectively connected to the power electronic switches S_1 and S_2. Since the voltage of the solar cell array is lower than that of the battery set, S_1 should further contain a diode to form a unidirectional switch to prevent the battery voltage from affecting the voltage of the solar cell array. Power electronic switches S_1 and S_2 are used as switches during the buck mode.

For the proposed SPGS, the solar cell array and the battery set will not release the power at the same time; hence, the power electronic switches S_1 and S_2 will not operate at the same time. The DIBBDAI also includes a bridge structure that is composed of S_3-S_6 for commutation, in order to generate an AC output current. Among them, S_3 and S_4 further contain a diode to form a unidirectional switch to avoid short circuit in the grid. S_3 or S_4 are also used as switches during the boost mode. C_{f1}, C_{f2}, R_f and L_f create a damped second-order low-pass filter.

If the solar cell array is operating and the battery set is disabled, S_1 is activated and S_2 is turned off. If the grid has two DC input terminals, which are respectively connected to battery set and the solar cell array, and both the battery set and the solar cell array can directly use the DIBBDAI to convert DC power into AC power for supplying to the grid.

When the output power from the solar cell array is stable, the DIBBDAI converts the power from the solar cell array to the grid, so the BPC is disabled and the battery set is in stand-by mode. The DIBBDAI converts the power from the battery set to the grid when the power of solar cell array suddenly decreases, and the BPC tracks the maximum power of solar cell array to charge the battery set. When the power of solar cell array suddenly increases, the DIBBDAI and voltage is lower than the voltage of the solar cell array, the DIBBDAI is operated in the buck mode. At this time, S_1 is operated in pulse width modulation (PWM) switching and S_3-S_6 are operated in accordance with the polarity of the grid voltage. The operation of buck mode can be divided into four modes.

Mode Bk-1: During the positive half cycle of the grid voltage, S_1, S_3, and S_6 are turned on, and S_4, S_5 and D are turned off. The change rate for the inductor current is:

$$\frac{di_L}{dt} = \frac{V_{sol} - v_s}{L} \tag{1}$$

where v_s and V_{sol} are the grid voltage and the voltage of the solar cell array, respectively. The solar cell array releases energy to the inductor and the grid.

Mode Bk-2: During the positive half cycle of the grid voltage, S_3, S_6 and D are turned on, and S_1, S_4, and S_5 are turned off. The change rate for the inductor current is:

$$\frac{di_L}{dt} = -\frac{v_s}{L} \tag{2}$$

The inductor releases energy to the grid.

Mode Bk-3: During the negative half cycle of the grid voltage, S_1, S_4 and $S_5$are turned on, and S_3, S_6 and D are turned off. The change rate for the inductor current is:

$$\frac{di_L}{dt} = \frac{V_{sol} + v_s}{L} \tag{3}$$

The solar cell array releases energy to the inductor and the grid.

Mode Bk-4: During the negative half cycle of the grid voltage, S_4, S_5 and D are turned on, and S_1, S_3 and S_6 are turned off. The change rate for the inductor current is:

$$\frac{di_L}{dt} = -\frac{v_s}{L} \tag{4}$$

The inductor releases energy to the grid.

The equivalent circuit for the DIBBDAI in the buck mode is shown in Fig. 2, where S is S_1. The grid voltage is converted

to its absolute value by the operation of S_3-S_6 and then added to the output of conventional buck power converter. As a result, the DIBBDAI operates as a conventional buck power converter, and the inductor current can be controlled by the switching of S.

If the grid voltage is higher than the voltage of the solar cell array, the DIBBDAI operates in the boost mode. At this time, S_1 is always on, S_4 and S_3 are respectively operated in PWM switching during the positive and negative half cycles for the grid voltage and S_6 and S_5 are operated in accordance with the polarity of the grid voltage. The operation of boost mode can also be divided into four modes.

Mode Bt-1: When the grid voltage is in the positive half cycle, S_3, S_4 and S_6 are turned on and S_5 is turned off. The change rate for the inductor current is:

$$\frac{di_L}{dt} = \frac{V_{sol}}{L} \tag{5}$$

The solar cell array releases energy to the inductor.

Mode Bt-2: When the grid voltage is in the positive half cycle, S_3 and S_6 are turned on and S_4 and S_5 are turned off. The change rate for the inductor current is:

$$\frac{di_L}{dt} = \frac{V_{sol} - v_s}{L} \tag{6}$$

Both the solar cell array and the inductor release energy to the grid.

Mode Bt-3: When the grid voltage is in the negative half cycle, S_3, S_4 and S_5 are turned on and S_6 is turned off. The change rate for the inductor current is:

$$\frac{di_L}{dt} = \frac{V_{sol}}{L} \tag{7}$$

The solar cell array releases energy to the inductor.

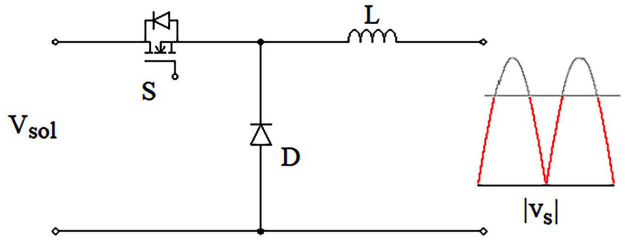

FIGURE 2. Equivalent circuit for the DIBBDAI in the buck mode.

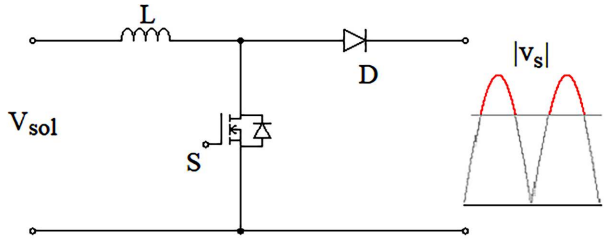

FIGURE 3. Equivalent circuit for the DIBBDAI in the boost mode.

Mode Bt-4: When the grid voltage is in the negative half cycle, S_4 and S_5 are turned on and S_3 and S_6 are turned off. The change rate for the inductor current is:

$$\frac{di_L}{dt} = \frac{V_{sol} + v_s}{L} \tag{8}$$

Both the solar cell array and the inductor release energy to the grid.

The equivalent circuit for the DIBBDAI operating in the boost mode is shown in Fig. 3. The grid voltage is converted to its absolute value and then added to the output of conventional BPC by the operation of S_3-S_6. In Fig. 3, switch S is S_4 or S_3 and the diode is the body diode of S_3 or S_4 depending on the polarity of the grid voltage. The DIBBDAI operates as a conventional BPC and the inductor current is controlled by switching S.

When the DIBBDAI is powered by the battery set, S_2 is activated and S_1 is turned off. At this time, the DIBBDAI operates similarly to when the solar cell array is operated, and it is not repeated.

The operation of S_1-S_6 is summarized in Tab. 1 where PHC and NHC mean the positive half cycle and negative half cycle. Fig. 4 shows the control signals S_1-S_6 and operation voltage during a grid cycle when the solar cell array supplies power to the DIBBDAI. As can be seen in Fig. 4, only one power electronic switch is operated in PWM switching at any time, and V_{AN} and V_{BN} are close to the positive cycle voltage and the negative cycle voltage of grid, respectively.

Fig. 5 shows the equivalent circuit of the DIBBDAI for the leakage current analysis [33], [34]. In Fig. 5, C_{pv} and R_g are the stray capacitor for the solar cell array and ground resistor for the grid, respectively. V_{AN} and V_{BN} are the voltages from terminals A and B to the negative terminal N of the solar cell array, respectively. Since C_{f1}, C_{f2} and R_f are connected across terminals A and B, these components do not affect the leakage current. S_5 and S_6 are switched synchronously with the grid voltage. S_6 is turned on and S_5 is turned off when the grid voltage is in the positive half cycle, and:

$$V_{AN} = v_s + v_{Lf} \tag{9}$$

$$V_{BN} = 0 \tag{10}$$

where v_{Lf} is the voltage of L_f. Since V_{BN} is equal to 0, the voltage across the loop of C_{PV} and R_g is 0 and the leakage current is 0.

When the grid voltage is in the negative half cycle, S_5 is turned on and S_6 is turned off and

$$V_{AN} = 0 \tag{11}$$

$$V_{BN} = -(v_s + v_{Lf}) \tag{12}$$

The voltage across the loop of C_{PV} and R_g is $-(v_s + v_{Lf})$. Since v_s is a sinusoidal voltage of 60Hz and the impedance of the stray capacitor is very large at 60Hz, the leakage current induced by v_s is very small. v_{Lf} contains a switching-frequency component, which is caused by the switching-frequency ripple in the output current. However, the switching-frequency component of v_{Lf} is effectively suppressed by C_{f1}, C_{f2} and R_f. As can be seen in

TABLE 1. Operation of S_1-S_6.

	power source	voltage range	S_1	S_2	S_3	S_4	S_5	S_6
PHC	solar cell array	$v_S<V_{sol}$	PWM	off	on	off	off	on
		$v_S>V_{sol}$	on	off	on	PWM	off	on
	battery	$v_S<V_b$	off	PWM	on	off	off	on
		$v_S>V_b$	off	on	on	PWM	off	on
NHC	solar cell array	$\|v_S\|<V_{sol}$	PWM	off	off	on	on	off
		$\|v_S\|>V_{sol}$	on	off	PWM	on	on	off
	battery	$\|v_S\|<V_{sol}$	off	PWM	off	on	on	off
		$\|v_S\|>V_{sol}$	off	on	PWM	on	on	off

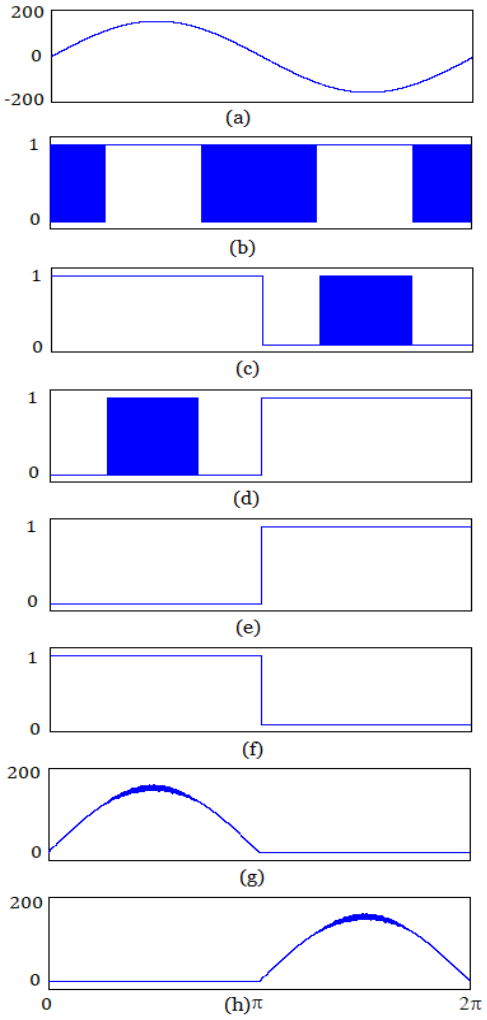

FIGURE 4. Control signals S_1-S_6 and operation voltage in a power grid cycle, (a) utility voltage, (b) S_1, (c) S_3, (d) S_4, (e) S_5, (f) S_6, (g) V_{AN}, (h) V_{BN}.

Fig. 4 (g) and (h), V_{AN} and V_{BN} are respectively close to the positive cycle voltage and the negative cycle voltage of grid, and it is consistent with the analysis. Accordingly, the leakage current induced by v_{Lf} is still small even the impedance of the stray capacitor at the switching frequency is small. Therefore, the leakage current contains a small switching-frequency component and a small fundamental component during the negative half cycle.

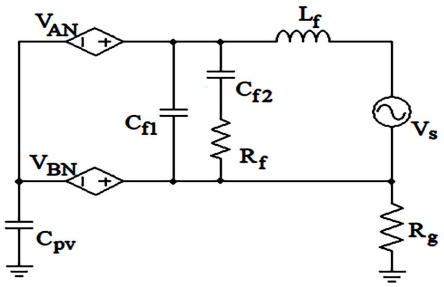

FIGURE 5. Equivalent circuit of the DIBBDAI for the leakage current analysis.

IV. OPERATION OF BPC

The BPC is inserted between the solar cell array and the battery set and is used when the battery set is charged by the solar cell array. The BPC is disabled when the power variation for the solar cell array is within the specified range. The BPC performs maximum power tracking (MPPT) for the solar cell array if the power variation for the solar cell array exceeds the specified range. The BPC is designed to be operated in continuous-conduction mode, and the relationship between the voltage of the solar cell array and the voltage of the battery set is:

$$\frac{V_{sol}}{V_{bat}} = \frac{1}{1 - D_{Sb}} \tag{13}$$

where D_{Sb} is the duty cycle for S_b.

V. SMOOTHING OPERATION

If the output power of the solar cell array is stable, the output power from the solar cell array is converted into AC power by the DIBBDAI. At this time, the DIBBDAI performs MPPT using the perturbation and observation (P&O) method. The output voltage from the solar cell array is disturbed, and then the change in the power from the solar cell array is observed to determine the direction in which the output voltage from the solar cell array is disturbed until the maximum power point is tracked. The output power smoothing mechanism is activated when the power variation for the solar cell array significantly exceeds the specified range. The state of charge (SOC) of the battery set is specified as between 30% and 90% to avoid over-charging or over-discharging, which decreases the life of the battery set. Considering the upward and downward power fluctuations of SPGS, the desired SOC of the battery set is at 60% when the battery set is in the stand-by mode. Since this study concerns the smoothing operation for the output power from the SPGS, the SOC of the battery set is estimated simply using the terminal voltage.

The output power from the SPGS is smoothed when the power variation (ΔP_{PV}) for the solar cell array exceeds the specified value P_1. P_1 is determined by the power variation of regulation. The DIBBDAI is still powered by the solar

cell array but MPPT is performed by the BPC using the P&O method. Consequently, the output current amplitude of DIBBDAI is controlled to be increased linearly along a specified gradient, driving the output power (P_{out}) from the SPGS also linearly increases along the specified gradient. The specified gradient for the output current amplitude depends on the allowable maximum power variation for P_{out}. At this time, the difference between the P_{PV} and P_{out} is positive. This power difference is automatically injected into the battery set through the BPC and the SOC of battery set is increased. When P_{out} exceeds P_{PV} by P_2, the DIBBDAI controls the output current amplitude to be a fixed value. The BPC still performs MPPT. At this time, the difference between P_{PV} and P_{out} becomes negative and the power difference is automatically supplied from the battery set to decrease the SOC of the battery set. If P_{PV} remains stable, the BPC stops operating when the SOC of the battery decreases to 60%. The DIBBDAI performs MPPT. At this moment, the power variation in P_{out} is P_2. P_2 must be less than or equal to P_1 to avoid exceeding the power variation of regulation. When the output power P_{out} is still less than P_{PV} and the SOC of the battery set has been equal to 90%, the BPC stops and the power smoothing function is disabled, in order to prevent the battery set from over-charging.

The output power from the SPGS is also smoothed when ΔP_{PV} for the output power from the solar cell array decreases to less than the specified value $-P_1$. At this time, the DIBBDAI is powered by the battery set and the BPC performs MPPT. The solar cell array charges the battery set through the BPC. The DIBBDAI decreases the amplitude of the output along the specified gradient, so P_{out} also linearly decreases along the specified gradient. At this time, the difference between P_{out} and P_{PV} is automatically supplied from the battery set and the SOC of the battery set is decreased. When P_{out} is P_1 less than P_{PV}, the DIBBDAI maintains the output current amplitude at a fixed value. The BPC continuously performs MPPT. P_{PV} is greater than P_{out} so the battery set is charged instead and the SOC of the battery set is increased. If P_{PV} remains stable, the BPC stops operating when the SOC of the battery is increased to 60%. The DIBBDAI is powered by the solar cell array and performs MPPT. At this moment, the power variation in P_{out} is P_2. If P_{out} is not less than P_{PV} and the SOC of the battery set has been equal to 30%, the BPC stops smoothing the power output of the SPGS, in order to prevent the battery set from over-discharging. The DIBBDAI is powered by the solar cell array and performs MPPT.

The operation flowchart for the proposed SPGS with power smoothing function is shown in Fig. 6. No matter P_{PV} increases or decreases drastically, P_{out} increases or decreases linearly along the specified gradient to smooth the output power from the SPGS. Since the battery set is actuated only when the absolute value of power variation (ΔP_{PV}) for the solar cell array exceeds the specified value P_1, the charging/discharging time of the battery set is much less than other smoothing methods [3]–[9]. Moreover, regardless of whether the battery set is charged or discharged to smooth the output power from the solar cell array, the battery set will immediately discharge or charge to maintain its SOC close to 60% when P_{out} catches up with P_{PV}. As a result, the capacity of battery set can be reduced.

VI. CONTROL BLOCK

Fig. 7 shows the control block for the DIBBDAI. The output voltage and the output current from the solar cell array are sent to the MPPT block to calculate P_{PV} and to generate a predicted voltage for the solar cell array. The predicted voltage and the detected voltage for the solar cell array are sent to a proportional integral (PI) controller to generate a MPPT control signal. The power variation (ΔP_{PV}) for the solar cell array is also calculated in the MPPT block. ΔP_{PV} is sent to comparison block I and compared with (P_1, $-P_1$) to generate an amplitude gradient control signal, S_{sl}. When $P_{PV} > P_1$, S_{sl} is $+V_{sl}$. S_{sl} is $-V_{sl}$ when $\Delta P_{PV} < -P_1$. When ΔP_{PV} is between P_1 and $-P_1$, S_{sl} is 0. S_{sl} is sent to an integrator. When S_{sl} is $+V_{sl}$, a linearly increasing signal is generated. A linearly decreasing signal is generated if S_{sl} is $-V_{sl}$. Therefore, V_{sl} controls the gradient of the amplitude control signal for the output current to determine the gradient in P_{out} when the smoothing function is actuated. When P_{PV} is stable, S_{sl} is 0 and the amplitude control signal is determined by the MPPT control signal. The MPPT control signal remains unchanged and V_{sl} controls the gradient of the amplitude control signal for the output current if P_{PV} changes significantly. The amplitude control signal and a unity sinusoidal signal are sent to a multiplier and an absolute value block to generate the output current reference signal. The unity sinusoidal signal is generated by a phase-locked loop (PLL) and a sinusoidal table to ensure the unity sinusoidal signal is a sine-wave and in phase with the grid voltage. Because the DIBBDAI can be operated in the buck mode and the boost mode, the current control involves two parts. The detected output current is sent to an absolute value block. In buck mode, the detected absolute output current is compared with the output current reference signal and sent to the current controller I. The output from current controller I is added to the feedforward control signal $v_{f,bk}$ to generate a buck modulation signal and then sent to the PWM block I. to generate a buck PWM signal PWM_{bk}. The carrier based PWM technology is used in the PWM block I. The buck modulation signal is compared with a triangle carrier in the PWM block I to generate a buck PWM signal PWM_{bk}. The feedforward control signal $v_{f,bk}$ is:

$$v_{f,bk} = \frac{|v_s|}{k_{pwm1}} \tag{14}$$

and,

$$k_{pwm1} = \frac{V_{dc}}{V_{tri}} \tag{15}$$

where V_{tri} is the peak value for the triangular carrier and V_{dc} is the input voltage for the DIBBDAI, which is the voltage of either the solar cell array or the battery set.

Since the output current from the DIBBDAI contains large high-frequency switching harmonics in the boost mode, the

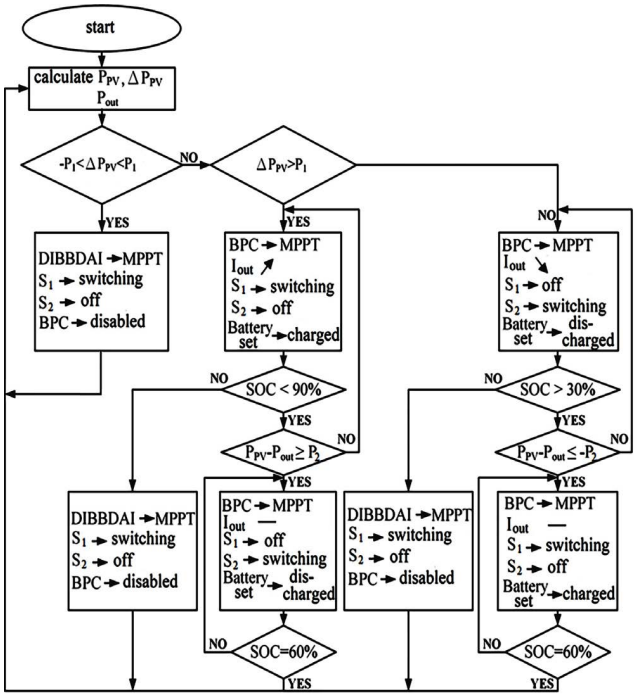

FIGURE 6. Operation flowchart for the proposed SPGS with power smoothing function.

detected absolute output current is sent to an extra low-pass filter. The output from the low-pass filter is compared with the output current reference signal and then sent to the current controller II. The output from the current controller II is added to the feedforward control signal $v_{f,bt}$ to generate a boost modulation signal and then sent to the PWM block II. The carrier based PWM technology is also used in the PWM block II. The boost modulation signal is compared with a triangle carrier in the PWM block II to generate a boost PWM signal PWM_{bt}. The feedforward control signal $v_{f,bt}$ is:

$$v_{f,bt} = \frac{|v_s| - V_{dc}}{|v_s|} V_{tri} \tag{16}$$

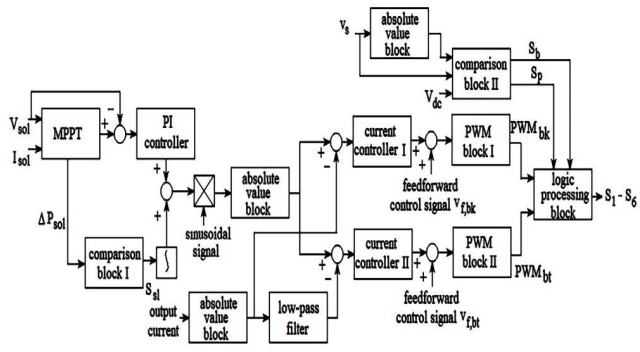

FIGURE 7. Control block for the DIBBDAI.

The feedforward control signals $v_{f,bk}$ and $v_{f,bt}$ will generate the major part of modulation signal, and the current controller I and the current controller II are used to fine tune the modulation signal to ensure that the detected absolute output current can trace the output current reference signal to be an absolute sine-wave.

TABLE 2. Circuit parameters of the prototype.

BPC			
L_b	1mH	switching frequency	20kHz
DIBBDAI			
L	1mH	switching frequency	20kHz
C_{f1}, C_{f2}	9.4μF	L_f	0.5mH
C_b, C_s	1000μF		

The grid voltage is sent to the comparison block II and compared with 0 to generate a control signal, S_p. S_p is 1 and 0 during the positive and negative half cycles of the grid voltage, respectively. The absolute value of the grid voltage is also compared with V_{dc} to generate a control signal, S_b. When the absolute value of the grid voltage is greater than V_{dc}, S_b is 1, and the DIBBDAI operates in the boost mode. On the contrary, S_b is 0, and the DIBBDAI operates in the buck mode. Finally, S_p, S_b, PWM_{bk} and PWM_{bt} are sent to the logic processing block to create the control signals for S_1-S_6. The control signals for S_1-S_6 are:

$$S_1 = (\bar{S}_b PWM_{bk} + S_b) \cdot S_o \tag{17}$$
$$S_2 = (\bar{S}_b PWM_{bk} + S_b) \cdot \bar{S}_o \tag{18}$$
$$S_3 = \bar{S}_p \cdot S_b \cdot PWM_{bt} + S_p \tag{19}$$
$$S_4 = S_p \cdot S_b \cdot PWM_{bt} + \bar{S}_p \tag{20}$$
$$S_5 = \bar{S}_p \tag{21}$$
$$S_6 = S_p \tag{22}$$

where S_o depends on the input source for the DIBBDAI. S_o is 1 if the solar cell array provides power and 0 if the battery set provides power.

The BPC is controlled by current control, which uses the MPPT control signal from the solar cell array and the current from the inductor L_b, and the output of current control is sent to the PWM block to create the control signal for S_D.

VII. EXPERIMENTAL RESULTS

To verify the performance of the proposed SPGS, an 800VA prototype was created for practical experiments. Fig. 8 is the prototype of proposed SPGS. The circuit parameters for the prototype are shown in Tab. 2. The prototype is connected to a single-phase utility that operates at 110V and 60Hz. The battery set contains ten batteries connected in series, and the nominal voltage of battery is 12V.

In order to facilitate the experiments, the solar cell array is replaced with a power supply for steady-state test. Fig. 9 shows the experimental results for the DIBBDAI. The output voltage from the power supply is 100V. Fig. 9(b) shows that the output current for the DIBBDAI is a sine wave that is in phase with the grid voltage. Fig. 9(c) shows that the current for the inductor L is similar to the output current in buck mode. However, the current for the inductor L and the output current have a relationship of (1-D) times in boost

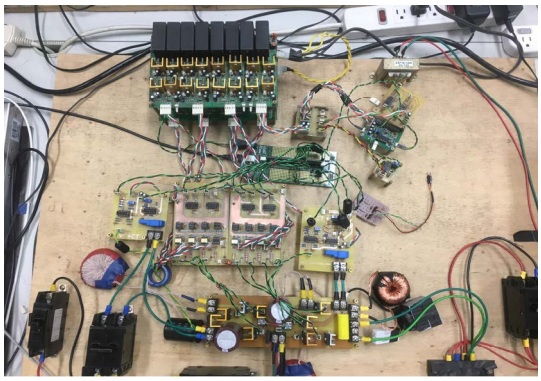

FIGURE 8. Prototype of the proposed SPGS.

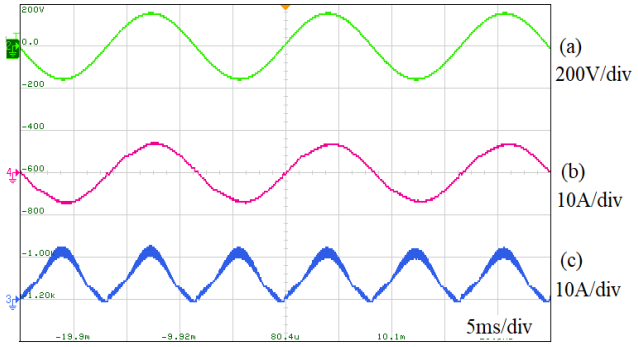

FIGURE 9. Experimental results of the DIBBDAI under steady state, (a) grid voltage, (b) output current, (c) inductor L current.

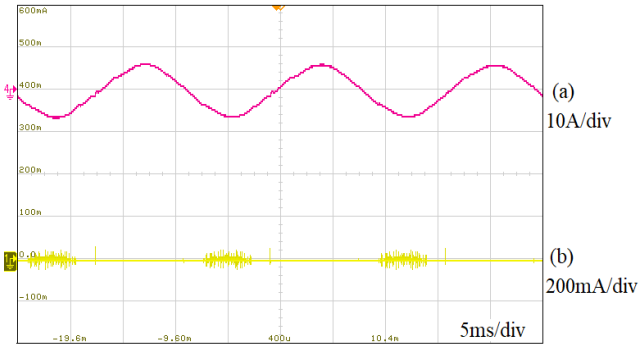

FIGURE 10. Experimental results for the leakage current of DIBBDA, (a) output current, (b) leakage current.

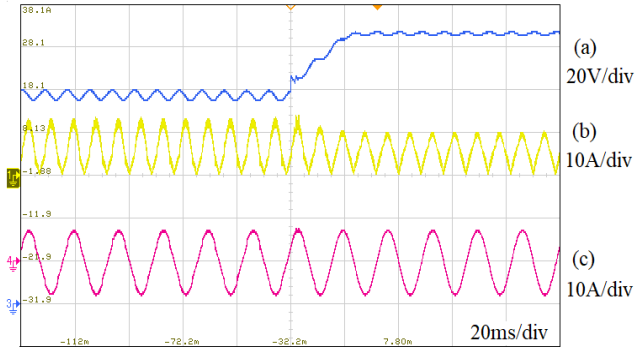

FIGURE 11. Experimental results for the variation of input DC voltage, (a) input DC voltage, (b) inductor L current, (c) output current.

mode, where D is the duty cycle of S in the equivalent circuit for the boost mode. Since D is not a constant, the relationship between the current for inductor L and the output current is nonlinear. Fig. 10 shows the experimental results for the leakage current for the DIBBDA. A capacitor of 60nF and a resistor of 5Ω are respectively used to simulate the stray capacitance for the solar cell array and the ground resistor for the grid. Fig. 10 shows that the leakage current is almost zero during the positive half cycle for the grid and there is a small high-frequency component in the leakage current during the negative half cycle for the grid. These experimental results are consistent with the analysis in Sec. III. The RMS value of the leakage current is 10.15mA in Fig. 10.

Since the DIBBDA can be powered by the solar cell array or the battery set, the input DC voltage will be changed instantly when the input power source is changed. Fig. 11 shows the experimental results when the input DC voltage for the DIBBDA is changed. In order to facilitate the observation of the impact on the input DC voltage change, the input power source is not changed but the input DC voltage is changed from 87V to 125V. Fig 11(c) shows that the output current from the DIBBDA is almost unaffected by a change in the input DC voltage. However, the maximum value for the current of inductor L, which is shown in Fig. 11(b), is reduced because the interval for the boost mode decreases. Fig. 12 shows the experimental results for the BPC, where the solar cell array charges the battery set. Fig. 13 shows the power efficiency of the DIBBDA for different input DC voltages. The higher the input DC voltage is, the higher the power efficiency of DIBBDA will be.

The solar cell array is composed of three solar modules connected in series. The maximum power, open-circuit voltage and short-circuit current of solar module are 255W, 38.08V and 8.65A, respectively. The PV simulator is used in the experiments, and the setting of PV simulator is according to the practical solar cell array. Fig. 14 shows the output power from the solar cell array where the short-current is set at about 6A to simulate 700W/m^2 illumination. Fig. 14(a) shows the power sweep curve of the solar cell array, where the voltage of solar cell array changes with time. As can be seen, the maximum power is about 550W. Fig. 14(b) shows the output power from the solar cell array when the solar cell array is connected to the input of the DIBBDA. From Fig 14(b), it is seen that the output power from the solar cell array gradually increased, and finally maintained at 550W. This proves the MPPT performance of the DIBBDA. Figs. 15 and 16 show the transient results when the power variation for the solar cell array significantly exceeds the specified value. The parameters P_1 and P_2 in the operation flowchart are 80W/min and 65W, respectively. In Fig. 15, the output power from the solar cell array is suddenly increased from 300W to 500W. As can be seen, the output power from the SPGS increases along the specified gradient and excess

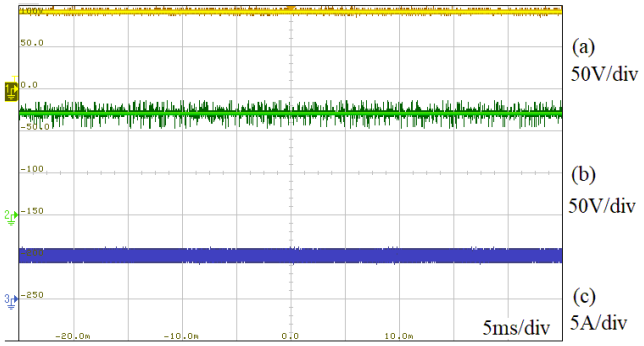

FIGURE 12. Experimental results for the BPC, (a) solar cell array voltage, (b) battery set voltage, (c) inductor L_b current.

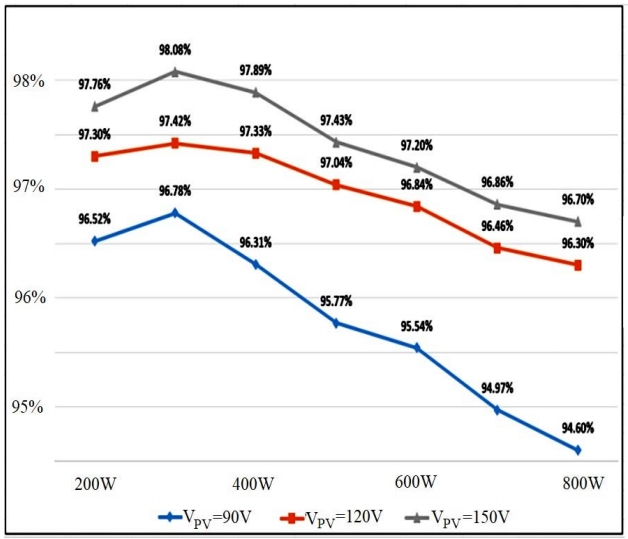

FIGURE 13. Power efficiency for the DIBBDA under different input DC voltages.

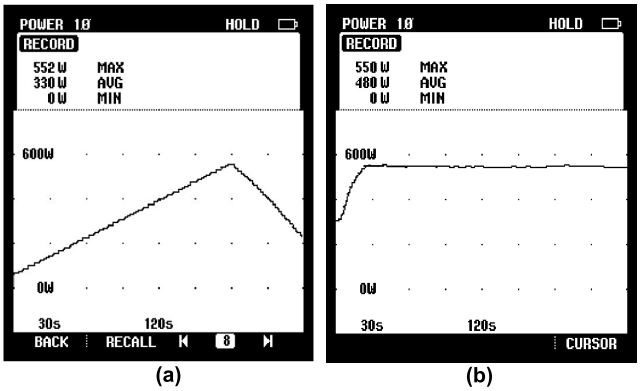

FIGURE 14. Output power from the solar cell array, (a) power sweep curve, (b) MPPT process.

power from the solar cell array will charge the battery set. The specified gradient for the output power from the SPGS is about 80W/min, which equates to a 10% variation in the rated power per minute. The output power from the SPGS is

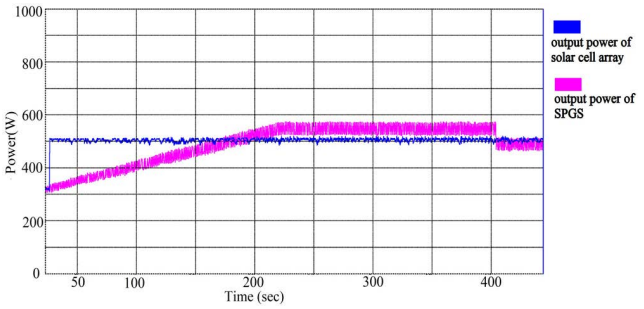

FIGURE 15. Transient result for suddenly increasing the output power from the solar cell array.

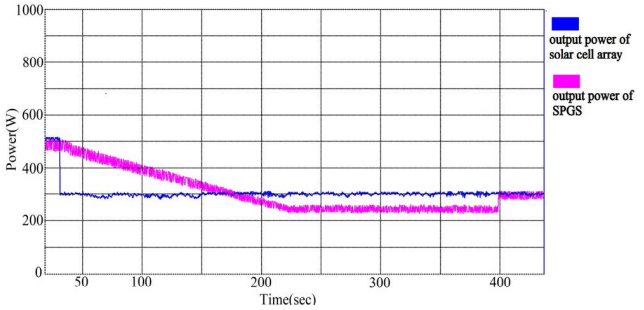

FIGURE 16. Transient result for suddenly decreasing the output power from the solar cell array.

increased to more than the output power from the solar cell array by the setting power P_2 so as to discharge the battery set. The output power from the SPGS then decreases to be close to the output power from the solar cell array when the discharging power is almost equal to the charging power for the battery set. In Fig. 16, the output power from the solar cell array is suddenly decreased from 500W to 300W. As can be seen, the output power from the SPGS decreases along the specified gradient, and the insufficient power will be discharged from the battery set. The output power from the SPGS decreases to less than the output power from the solar cell array by the setting power P_2 so as to charge the battery set. The output power from the SPGS then increases to be close to the output power from the solar cell array when the charging power is almost equal to the discharging power for the battery set.

VIII. CONCLUSION

This study proposes a SPGS with a power smoothing function. The proposed SPGS uses a DIBBDAI to integrate the solar cell array and the battery set for outputting a smoother power. The proposed SPGS has the following innovative features.

1. The SPGS integrates two input power sources, solar cell array and battery set, which can be changed seamlessly. The battery set acts as an energy buffer to smooth the power variation from the SPGS. The proposed SPGS using only two power stages, hence, the power circuit is simplified.

2. Regardless of whether the input power source is the solar cell array or the battery set, only one power stage is required to convert DC power to AC power. Besides, the power for charging the battery set from the solar cell array is only through one power stage.
3. The leakage current induced by the stray capacitance of the solar cell array is suppressed due to the use of the proposed SPGS.

The experimental results show that the proposed SPGS outputs a sinusoidal current in phase with the utility voltage and smooth the power variation caused by the power fluctuation from the solar cell array. In addition, the leakage current of solar cell array is effectively suppressed. Therefore, it verifies that the major concerns of power fluctuation and leakage current can be solved by using the proposed SPGS. An evaluation for the capacity of battery set required for smoothing and comparison with other smoothing methods in the practical application will be further studied in the future.

REFERENCES

[1] Q. Peng, A. Sangwongwanich, Y. Yang, and F. Blaabjerg, "Grid-friendly power control for smart photovoltaic systems," *Sol. Energy*, vol. 210, pp. 115–127, Nov. 2020.

[2] D. Cheng, B. A. Mather, R. Seguin, J. Hambrick, and R. P. Broadwater, "Photovoltaic (PV) impact assessment for very high penetration levels," *IEEE J. Photovolt.*, vol. 6, no. 1, pp. 295–300, Jan. 2016.

[3] J. Martins, S. Spataru, D. Sera, D.-I. Stroe, and A. Lashab, "Comparative study of ramp-rate control algorithms for PV with energy storage systems," *Energies*, vol. 12, no. 7, p. 1342, Apr. 2019.

[4] D. Lin and N. Normal University, "Strategy comparison of power ramp rate control for photovoltaic systems," *CPSS Trans. Power Electron. Appl.*, vol. 5, no. 4, pp. 329–341, Dec. 2020.

[5] H. Nazaripouya, C.-C. Chu, H. R. Pota, and R. Gadh, "Battery energy storage system control for intermittency smoothing using an optimized two-stage filter," *IEEE Trans. Sustain. Energy*, vol. 9, no. 2, pp. 664–675, Apr. 2018.

[6] K. Koiwa, K.-Z. Liu, and J. Tamura, "Analysis and design of filters for the energy storage system: Optimal tradeoff between frequency guarantee and energy capacity/power rating," *IEEE Trans. Ind. Electron.*, vol. 65, no. 8, pp. 6560–6570, Aug. 2018.

[7] M. J. E. Alam, K. M. Muttaqi, and D. Sutanto, "A novel approach for ramp-rate control of solar PV using energy storage to mitigate output fluctuations caused by cloud passing," *IEEE Trans. Energy Convers.*, vol. 29, no. 2, pp. 507–518, Jun. 2014.

[8] A. Atif and M. D. Khalid, "Saviztky-Golay filtering for solar power smoothing and ramp rate reduction based on controlled battery energy storage," *IEEE Access*, vol. 8, pp. 33806–33817, 2020.

[9] M. A. Syed and M. Khalid, "Moving regression filtering with battery state of charge feedback control for solar PV firming and ramp rate curtailment," *IEEE Access*, vol. 9, pp. 13198–13211, 2021.

[10] M. J. E. Alam, K. M. Muttaqi, and D. Sutanto, "Battery energy storage to mitigate rapid voltage/power fluctuations in power grids due to fast variations of solar/wind outputs," *IEEE Access*, vol. 9, pp. 12191–12202, 2021.

[11] A. Makibar, L. Narvarte, and E. Lorenzo, "Contributions to the size reduction of a battery used for PV power ramp rate control," *Sol. Energy*, vol. 230, pp. 435–448, Dec. 2021.

[12] M. Combe, A. Mahmoudi, M. H. Haque, and R. Khezri, "Optimal sizing of an AC-coupled hybrid power system considering incentive-based demand response," *IET Gener., Transmiss. Distrib.*, vol. 13, no. 15, pp. 3354–3361, Jul. 2019.

[13] V. T. Tran, M. R. Islam, D. Sutanto, and K. M. Muttaqi, "Mitigation of solar PV intermittency using ramp-rate control of energy buffer unit," *IEEE Trans. Energy Convers.*, vol. 34, no. 1, pp. 435–449, Mar. 2019.

[14] S. Kumar, L. N. Patel, B. Singh, and A. L. Vyas, "Self-adjustable step-based control algorithm for grid-interactive multifunctional single-phase PV-battery system under abnormal grid conditions," *IEEE Trans. Ind. Appl.*, vol. 56, no. 3, pp. 2978–2987, May 2020.

[15] R. K. Dhar, A. Merabet, A. Al-Durra, and A. M. Y. M. Ghias, "Power balance modes and dynamic grid power flow in solar PV and battery storage experimental DC-link microgrid," *IEEE Access*, vol. 8, pp. 219847–219858, 2020.

[16] N. Vazquez, S. S. Yu, T. K. Chau, T. Fernando, and H. H.-C. Iu, "A fully decentralized adaptive droop optimization strategy for power loss minimization in microgrids with PV-BESS," *IEEE Trans. Energy Convers.*, vol. 34, no. 1, pp. 385–395, Mar. 2019.

[17] C. M. Nirmal Mukundan, P. Jayaprakash, U. Subramaniam, and D. J. Almakhles, "Binary hybrid multilevel inverter-based grid integrated solar energy conversion system with damped SOGI control," *IEEE Access*, vol. 8, pp. 37214–37228, 2020.

[18] J. Wu, H. Jou, and X. Wu, "Power conversion interface with harmonic suppression for a DC grid and single-phase utility," *IET Power Electron.*, vol. 13, no. 7, pp. 1302–1310, May 2020.

[19] D. Ghaderi, G. Bayrak, and J. M. Guerrero, "Grid code compatibility and real-time performance analysis of an efficient inverter topology for PV-based microgrid applications," *Int. J. Electr. Power Energy Syst.*, vol. 128, Apr. 2021, Art. no. 106712.

[20] E. Kabalcè, "Review on novel single-phase grid-connected solar inverters: Circuits and control methods," *Sol. Energy*, vol. 198, pp. 247–274, Mar. 2020.

[21] A. Sangwongwanich, Y. Yang, and F. Blaabjerg, "A sensorless power reserve control strategy for two-stage grid-connected PV systems," *IEEE Trans. Power Electron.*, vol. 32, no. 11, pp. 8559–8569, Nov. 2017.

[22] A. Sinha, K. C. Jana, and M. K. Das, "Control strategy of PV-fed, grid-interfaced, seven-level T-type MLI for distributed power generation," *IET Power Electron.*, vol. 12, no. 12, pp. 1–12, Jul. 2019.

[23] J. C. Wu, H. L. Jou, and P. H. Huang, "Seven-level power conversion system for solar power generation system," *IET Renew. Power Gener.*, vol. 14, no. 8, pp. 1387–1394, Jun. 2020.

[24] Y. He, Y. Xu, and J. Chen, "New space vector modulation strategies to reduce inductor current ripple of Z-source inverter," *IEEE Trans. Power Electron.*, vol. 33, no. 3, pp. 2643–2654, Mar. 2018.

[25] W. Xu, M. Liu, J. Liu, K. W. Chan, and K. W. E. Cheng, "A series of new control methods for single-phase Z-source inverters and the optimized operation," *IEEE Access*, vol. 7, pp. 113786–113800, 2019.

[26] S. Huang, F. Tang, Z. Xin, Q. Xiao, and P. C. Loh, "Grid-current control of a differential boost inverter with hidden LCL filters," *IEEE Trans. Power. Electron.*, vol. 34, no. 1, pp. 889–903, Jan. 2019.

[27] W. Yao, Y. Xu, Y. Tang, P. C. Loh, X. Zhang, and F. Blaabjerg, "Generalized power decoupling control for single-phase differential inverters with nonlinear loads," *IEEE J. Emerg. Sel. Topics Power Electron.*, vol. 7, no. 2, pp. 1137–1151, Jun. 2019.

[28] A. A. Khan, Y. W. Lu, W. Eberle, L. Wang, U. A. Khan, M. Agamy, and H. Cha, "Single-stage bidirectional buck–boost inverters using a single inductor and eliminating the common-mode leakage current," *IEEE Trans. Power Electron.*, vol. 35, no. 2, pp. 1269–1281, Feb. 2020.

[29] A. A. Khan, Y. W. Lu, U. A. Khan, L. Wang, W. Eberle, and M. Agamy, "Novel transformerless Buck–Boost inverters without leakage current," *IEEE Trans. Ind. Electron.*, vol. 67, no. 12, pp. 10442–10454, Dec. 2020.

[30] U. A. Khan and J.-W. Park, "Full-bridge single-inductor-based buck–boost inverters," *IEEE Trans. Power Electron.*, vol. 36, no. 2, pp. 1909–1920, Feb. 2021.

[31] O. Husev, O. Matiushkin, C. Roncero-Clemente, F. Blaabjerg, and D. Vinnikov, "Novel family of single-stage buck–boost inverters based on unfolding circuit," *IEEE Trans. Power Electron.*, vol. 34, no. 8, pp. 7662–7676, Aug. 2019.

[32] O. Matiushkin, O. Husev, J. Rodriguez, H. Young, and I. Roasto, "Feasibility study of model predictive control for grid-connected twisted buck–boost inverter," *IEEE Trans. Ind. Electron.*, vol. 69, no. 3, pp. 2488–2499, Mar. 2022.

[33] M. N. H. Khan, M. Forouzesh, Y. P. Siwakoti, L. Li, T. Kerekes, and F. Blaabjerg, "Transformerless inverter topologies for single-phase photovoltaic systems: A comparative review," *IEEE J. Emerg. Sel. Topics Power Electron.*, vol. 8, no. 1, pp. 805–835, Mar. 2020.

[34] H. Sabry, Z. M. Mohammed, F. H. Nordin, N. H. N. Ali, and A. S. Al-Ogaili, "Single-phase grid-tied transformerless inverter of zero leakage current for PV system," *IEEE Access*, vol. 8, pp. 4361–4371, 2020.